Influences of nitrogen flow rate on the structures and properties of Ti and N co-doped diamond-like carbon films deposited by arc ion plating*

Zhang Lin(张 林)[a)b)†], Ma Guo-Jia(马国佳)[b)], Lin Guo-Qiang(林国强)[a)], Ma He(马 贺)[b)], and Han Ke-Chang(韩克昌)[a)]

[a)] *Key Laboratory for Material Modification by Laser, Ion and Electron Beams, Dalian University of Technology, Dalian* 116024, *China*
[b)] *Science and Technology on Power Beam Processes Laboratory, Beijing Aeronautical Manufacturing Technology Research Institute, Beijing* 100024, *China*

(Received 26 July 2013; revised manuscript received 22 September 2013; published online 10 February 2014)

In this paper, Ti–C–N nanocomposite films are deposited under different nitrogen flow rates by pulsed bias arc ion plating using Ti and graphite targets in the Ar/N_2 mixture gas. The surface morphologies, compositions, microstructures, and mechanical properties of the Ti–C–N films are investigated systematically by field emission scanning electron microscopy (FE-SEM), x-ray photoelectron spectroscopy (XPS), grazing incident x-ray diffraction (GIXRD), Raman spectra, and nano-indentation. The results show that the nanocrystalline Ti(C,N) phase precipitates in the film from GIXRD and XPS analysis, and Raman spectra prove the presence of diamond-like carbon, indicating the formation of nanocomposite film with microstructures comprising nanocrystalline Ti(C,N) phase embedded into a diamond-like matrix. The nitrogen flow rate has a significant effect on the composition, structure, and properties of the film. The nano-hardness and elastic modulus first increase and then decrease as nitrogen flow rate increases, reaching a maximum of 34.3 GPa and 383.2 GPa, at a nitrogen flow rate of 90 sccm, respectively.

Keywords: arc ion plating, Ti–C–N film, nitrogen flow rate, microstructure

PACS: 81.15.Jj, 68.55.–a, 68.60.Bs, 61.05.cj **DOI:** 10.1088/1674-1056/23/4/048102

1. Introduction

Ti-based compounds such as TiN, TiC, and TiCN films have been successfully applied to various tools and dies due to their superior mechanical properties in past decades.[1–3] In recent years, some researchers have synthesized Ti–C–N nanocomposite films with high C content comprised of nanocrystalline TiN or TiCN dispersed in an amorphous carbon matrix, which exhibit better performance than TiN and TiC films.[4–6] Therefore, the deposition of Ti and N co-doped amorphous carbon films has been intensively investigated to enhance hardness and tribological properties. However, the microstructure and performance of the Ti–C–N film are strongly dependent on the deposition method, film architecture, and composition. At present, most of the previous studies mainly focus on the effects of amorphous carbon content on the composition, structure, and properties of Ti–N–C nanocomposite film. Barshilia *et al.*[7] synthesized the superhardness TiN/a-C nanocomposite coatings by reactive magnetron sputtering at carbon content of 17 at.%. Martinez *et al.*[6] found the amount of amorphous carbon phase exerted a great influence on the mechanical and tribological properties of Ti–C–N films. Lu and Shen[8] described that Ti–C–N films with different amounts of C showed the nanostructure transition from solid solution to nanocomposite. Meanwhile, Lu *et al.*[4] and Chen *et al.*[9] reported that the film hardness values exhibited different trends with the increase of nitrogen flow. However, up to now, there still have been few systematic investigations about the influences of nitrogen flow rate on the structures and properties of Ti and N co-doped amorphous carbon films.

In this study, pulsed bias arc ion plating (PBAIP) with graphite and titanium targets is used to synthesize Ti and N co-doped DLC films under different nitrogen flow rates. The effects of nitrogen flow rate on the structure and mechanical properties are investigated. It is expected that the structure and mechanical properties of the Ti–C–N films deposited by PBAIP will be significantly influenced by the nitrogen flow rate.

2. Experiment

Ti and N co-doped DLC films were deposited on W6Mo5Cr4V2 high-speed steel and silicon wafer substrates by home-designed pulsed bias arc ion plating equipment (MMLab-Arc II). A high-purity (99.99%) graphite target and a metal (99.99%) titanium target were used as cathode arc evaporation sources and located on the opposite sides in the chamber. Two arc sources work simultaneously in a mixture gas of Ar and N_2. High-speed steel substrates with a size

*Project supported by the National Natural Science Foundation of China (Grant No. 51271047).
†Corresponding author. E-mail: linzh1817@gmail.com
© 2014 Chinese Physical Society and IOP Publishing Ltd

of ϕ20 mm×3 mm were polished to a mirror surface with a roughness value of below 100 nm. All substrates were ultrasonically cleaned in alcohol for 15 min, then blown dry and put on holders. The chamber was evacuated to a base pressure below 5.0×10^{-3} Pa. Before deposition, the substrates was preheated and maintained at 150°. Ar ion sputtering cleaning was processed for 10 min to remove undesirable oxide and contamination layers at a bias voltage of 900 V with duty cycle of 50%. During the deposition, argon and nitrogen are introduced into the chamber through a piezoelectric valve and mass flow controller, respectively. In order to improve the adhesion property, a Ti interlayer was first deposited for 10 min. Five groups of Ti–C–N films were deposited by adjusting the nitrogen flow rate to 30, 50, 70, 90, and 150 sccm respectively. Arc currents of Ti and graphite targets were kept constant at 100 A and 50 A, respectively. The magnitude, duty cycle, and frequency of the negative pulsed bias applied to the holders were −300 V, 40%, and 40 kHz, respectively. For each film, the deposition time was fixed at 60 min.

The morphologies of the films were observed by field emission scanning electron microscope (FE-SEM, JEM2010). The chemical compositions and chemical states of the films were analyzed by X-ray photoelectron spectroscopy (XPS) measurement with an AXIS ULTRADLD spectrometer using Al Kα 1486.6 eV. The crystal structure was characterized by grazing incident X-ray diffraction (GIXRD) analysis with Cu Kα radiation (D8 Discover). The diffraction patterns were recorded in detector scan mode at grazing incident angle of 1°. The microstructure was evaluated by an INNIA Raman spectrometer (using He–Ne laser with a wavelength of 632.8 nm operated at 35 mW). The surface hardness and modulus were measured using a nano-indentation system with a Berkovich diamond tip under a continuous stiffness method (MTS, Nano-indenter XP). The indentation penetration depth obtained for the Ti–C–N films was 250 nm. Each film on a high-speed steel substrate was measured at nine different positions in an array and then the values were averaged.

3. Results and discussion

3.1. Surface morphology

Figure 1 shows the SEM image of the Ti–C–N film deposited at an N_2 flow rate of 90 sccm, and the other films exhibit the similar surface morphology. The thickness of Ti–C–N film is around 350 nm. It can be seen that the film is uniform and dense. Some small particles with sizes of 0.1 μm–2 μm exist on the film surface, showing the typical characteristic of arc ion plating technique. Moreover, the elimination of macroparticles is realized by the pulsed bias and enhanced magnetic filtering system.[10,11]

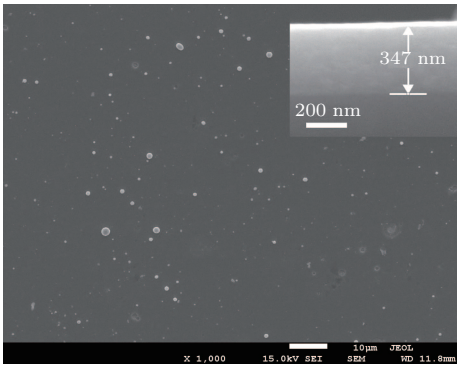


Fig. 1. Typical SEM image of Ti–C–N film deposited at an N_2 flow rate of 90 sccm.

3.2. Chemical composition

The wide scan spectrum of XPS results for the Ti–C–N film at a nitrogen flow rate of 70 sccm is given in Fig. 2. The C 1s, N 1s, and Ti 2p peaks are identified and the O 1s peak is also observed due to oxygen contamination of the environment. All high-resolution spectra of C 1s, N 1s, and Ti 2p are calibrated using the adventitious carbon C 1s peak with a binding energy of 284.8 eV. The film composition is calculated through subtracting the background from each spectrum and calculating the integral area using relative sensitivity factors of C (0.278), N (0.477), and Ti (2.001).

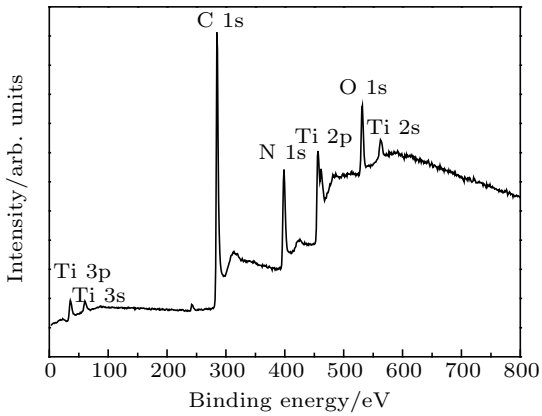


Fig. 2. XPS wide scan spectrum of the film deposited at a nitrogen flow rate of 70 sccm.

Figure 3 shows the variations of Ti, C, and N content with nitrogen flow rate. It can be seen that the N content first increases linearly from 12.2 at.% to 27.4 at.% as the nitrogen flow rate increases from 30 sccm to 70 sccm, then decreases gradually to 21.5 at.% at a nitrogen flow rate of 150 sccm. The Ti concentration exhibits a similar variation trend to N content. In the arc discharge process, Ar and N_2 in the chamber are ionized and used as working and reactive gases, respectively. The Ti–C–N film is produced by the reaction of C^+, N^+, and Ti^+ ions on the substrate surface. With the increase of nitrogen flow rate, more N^+ ions react with Ti^+ ions, and more N, Ti elements will be incorporated into the film, resulting in the increase of N and Ti content in the film. When nitrogen flow rate

exceeds a critical value of 70 sccm, the Ti and N content reduce simultaneously. A possible reason for this phenomenon is the decrease of the reactivity of ions in the plasma under high content of N_2. At a constant tall pressure, a higher N_2 flow rate corresponds to lower Ar partial pressure, thereby reducing the collision efficiency of the gases and reducing the activity of ions. On the other hand, the concentration of N–Ti bonds in the film decreases and more N–C bonds form, corresponding to the decrease and increase in Ti and C contents, respectively, which will be confirmed by the XPS analysis. In this study, the relative atomic ratio of $x = (C+N)/Ti$ varies from 2.4 to 4.7. The incorporation of more C atoms into the film is likely to promote the formation of a carbon matrix due to phase segregation.

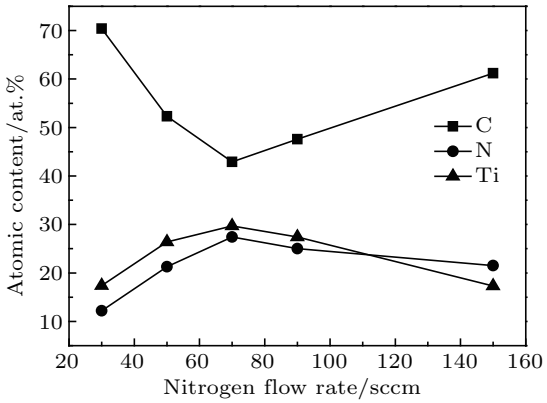


Fig. 3. Chemical compositions of Ti–C–N films versus nitrogen flow rate.

3.3. Chemical bonding

In order to characterize the chemical bonding structure, XPS analysis is carried out. Figure 4 depicts the high resolution C 1s, N 1s, and Ti 2p XPS spectra of the Ti–C–N films deposited with different N_2 flow rates. Figure 5 shows typical deconvolution results of C 1s, and N 1s XPS spectra of Ti–C–N film for 70 sccm. In Fig. 4(a), the main contribution of the C 1s appears at 284.8 eV, corresponding to the C–C bond. The lowest binding energy component located at 282 eV is assigned to the C–Ti bond. The C–Ti bonding energy of 282 eV is higher than that of the TiC/a-C film.[12] This is due to the formation of Ti(C,N) and the presence of the more electronegative nitrogen atoms in the local environment.[5] Hence, a certain amount of nanocrystalline phase existing in the film is actually Ti(C,N). According to the area of peak in Fig. 5(a), a small fraction of C atoms bond with Ti atoms compared with those bonding with C atoms (i.e., forming C–C bonds). The shoulder peak with a higher binding energy of 286.2 eV is associated with the C–N bond, which would influence the mechanical properties of the film.[6] In addition, the weak peak at the highest binding energy represents C–O bonds which is attributed to the contamination at the film surface due to the air exposure.[13]

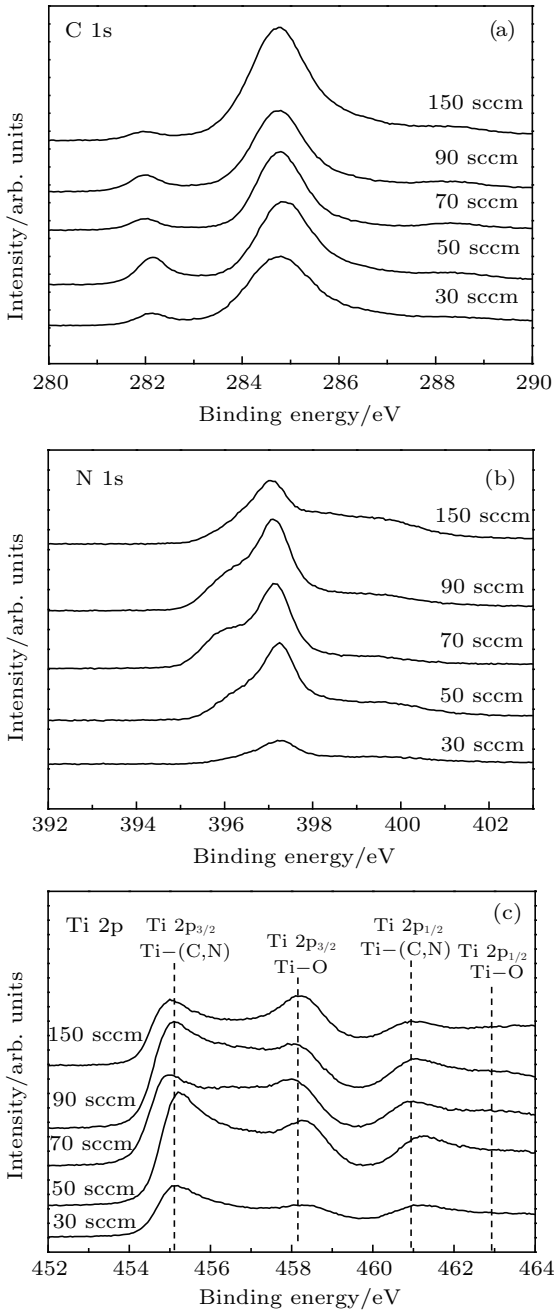


Fig. 4. C 1s (a), N 1s (b), and Ti 2p(c) core level spectra of the Ti–C–N films deposited at different N_2 flow rates.

In Fig. 4(b), N 1s XPS spectra each exhibit a high asymmetric feature, and there is a small charge shift towards lower binding energies as N_2 flow rate increases. Since the binding energy of N 1s spectrum for TiCN film is lower than that of TiN film, the peak shift is due to a large fraction of Ti(C,N) phases forming in the film.[14] The N 1s spectrum is de-convoluted into a main peak and two weak shoulder peaks as shown in Fig. 5(b). A main component at 397.1 eV corresponds to N–Ti bonds.[15] The first shoulder peak with a low binding energy of ∼396 eV is assigned to N–(Ti,O) bond.[16] The second shoulder peak at 398.7 eV could be attributed to sp^2 C–N bond.[13] The content values of N atoms with various

chemical states are calculated through the corresponding peak areas as shown in Table 1. It is found that the N–Ti bonds are the main components at low N_2 flow rates. With the further increase of N_2 flow rate, the fractions of N–Ti and N–(Ti,O) bonds decrease simultaneously, while sp^2 C–N bonds increase and finally dominate in the films at an N_2 flow rate of 150 sccm.

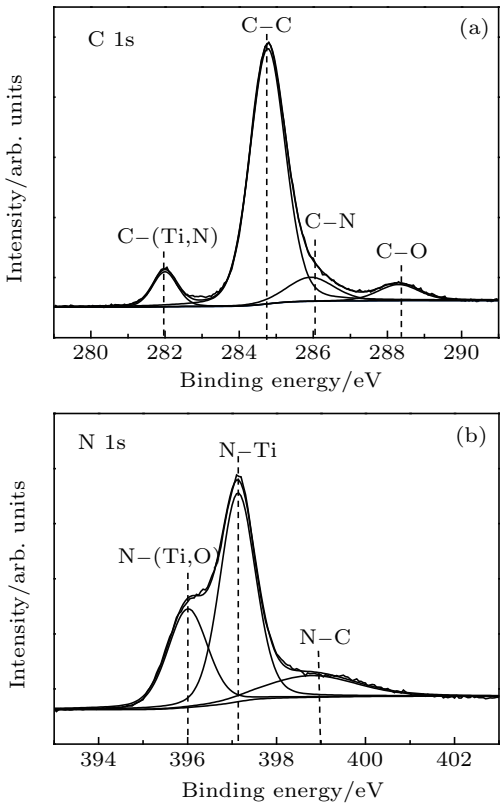


Fig. 5. Typical fitting curves of C 1s (a) and N 1s (b) of the Ti–C–N film at an N_2 flow rate of 70 sccm.

Table 1. Content values of N atoms with different chemical states.

N_2 flow rate/sccm	30	50	70	90	150
N–Ti/at.%	46.8	45.7	55.8	50.0	31.8
N–C/at.%	41.5	37.3	14.7	25.1	58.0
N–(Ti, O)/at.%	11.7	17.0	29.5	24.9	10.2

Figure 4(c) shows the peak positions of Ti 2p spectra. Ti 2p spectra each consist of four peaks. Two peaks appear at about 455.0 eV and 460.6 eV of binding energy, which are assigned, respectively, to the Ti $2p_{3/2}$ and Ti $2p_{1/2}$ photoelectron peaks corresponding to Ti–N or Ti–C bonds, and the other two peaks correspond to Ti–O bonds at 458.1 eV (Ti $2p_{3/2}$) and 463.1 eV (Ti $2p_{1/2}$) respectively. The presence of Ti–O bonds in the film is due to the surface contamination by oxygen adsorption into the films from air. The peak positions of Ti–N and Ti–C bonds can be hardly discriminated due to the fact that their binding energy is nearly identical to each other. However, combining with the observable peak information about C–(Ti,N) bonds in C 1s spectra and N–Ti bonds in N 1s spectra, it can be confirmed that the peaks located at 455.0 eV and 460.6 eV are assigned to Ti–(C,N) bonds. Therefore, it can be deduced that the $TiC_{1-x}N_x$ phases form in the films.

3.4. Microstructure

In order to investigate the crystalline structures of the Ti–C–N films, XRD is used. Figure 6 shows the grazing incident X-ray diffraction patterns of the Ti–C–N films deposited under different nitrogen flow rates. The diffraction peak of about 44.8° is assigned to the Fe (110) phase from the high-speed steel substrate. It is obvious that three peaks are identified at the diffraction angles (2θ) of 36.1°, 42.2°, and 61.4°, corresponding to the (111), (200), and (220) planes of fcc TiN phase, respectively. Nevertheless, the diffraction peaks shift towards low angles compared with those in standard spectra. This can be interpreted as the fact that ternary $TiC_{1-x}N_x$ phase may be formed. However, it is difficult to distinguish the TiN and $TiC_{1-x}N_x$ phases due to the similar atomic radii of C and N.[17] Therefore, we can consider the two components as Ti(C,N) phases consisting of TiN and $TiC_{1-x}N_x$ phases. In addition, at low nitrogen flow rate, the Ti(C,N) (111) peak exhibits the high intensity, indicating that a bigger fraction of Ti(C,N) phase are formed and the film grows preferentially along the (111) orientation. At a higher nitrogen flow rate, the Ti(C,N) (111) orientation decreases gradually. It is mainly attributed to the decrease of mole fraction and lower crystalline degree of crystalline Ti(C,N) due to low Ti content. Additionally, it could also be because the excess carbon formed in an amorphous phase inhibits the growth of Ti(C,N) crystallites. Thus fine crystallite size can be obtained at a high nitrogen flow rate, which exhibits low intensity. All films exhibit broadened diffraction peaks of Ti(C,N), suggesting a possible fine crystallite size or some internal stresses in the Ti–C–N film. The crystallite size is also roughly calculated according to the Debye–Scherrer formula, which is in a range of 11 nm–19 nm.

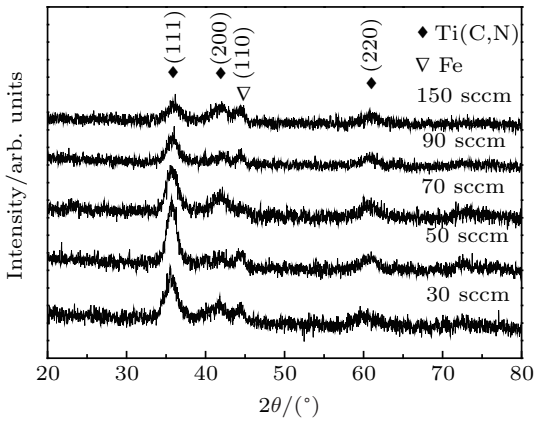


Fig. 6. GIXRD patterns of Ti–C–N films deposited at various nitrogen flow rates.

Figure 7 presents the Raman spectra corresponding to the Ti–C–N films with different nitrogen flow rates. For amor-

phous carbon or DLC films, the Raman spectrum typically shows a G peak centered around 1550 cm^{-1} and a D peak centered at 1360 cm^{-1}.[18] The G peak arises from the symmetric E_{2g} vibration mode, while the D peak corresponds to breathing modes of A_{1g} symmetry due to the disorder.[19] It is worth noting from this figure that there is an asymmetric broad peak between 1100 cm^{-1} and 1700 cm^{-1}, showing the characteristic peaks of a pure DLC film. Moreover, the signal feature of DLC becomes obvious as nitrogen flow rate increases, especially at a nitrogen flow rate of 150 sccm (seen from the insert in Fig. 7). Therefore, it can be concluded that the films prepared in our experiment are DLC-based composite films, which is indicated by a combination of GIXRD and XPS results. Normally, the Raman spectra of the DLC film can be fitted by the D peak and the G peak. It has been reported that the intensity ratio of I_D/I_G is proportional to the ratio of sp^2/sp^3 bonds, which is one of the most important factors determining the mechanical properties such as hardness.[20] However, the intensity of Raman spectrum in this study is relatively low due to the large volume of Ti(C,N) phase and small content of amorphous carbon. Thus, it is too difficult to fit by two Gaussian functions observed and calculate the intensity ratio of I_D/I_G.

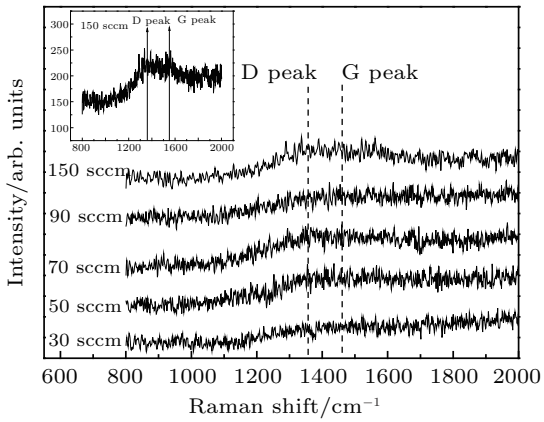


Fig. 7. Raman spectra of the Ti–C–N films prepared under different nitrogen flow rates.

3.5. Nano-hardness and elastic modulus

Figure 8 illustrates nano-hardness and elastic modulus values of the Ti–C–N films versus nitrogen flow rate. With the increase of nitrogen flow rate, the values of nano-hardness and elastic modulus increase linearly and reach their maximum values of 34.3 GPa and 383.2 GPa, respectively, at a nitrogen flow rate of 90 sccm. However, with the further increase of nitrogen flow rate, the values of nano-hardness and elastic modulus both decrease drastically. It is found from this figure that the nitrogen flow rate has a significant effect on the nano-hardness and elastic modulus of the Ti–C–N film. The Ti–C–N films prepared in our experiment are confirmed to be nanocomposite films by the Raman, GIXRD, and XPS analyses. The Ti(C,N) nanocrystallines are separated by an amorphous carbon matrix. Ti(C,N) nanocrystallines act as a reinforcing phase to improve mechanical properties, while amorphous carbon or carbonitride acts as a hard, tough, and lubricating matrix. As nitrogen flow rate increases, more Ti(C,N) nanocrystallines are formed and imbedded in the DLC matrix, which causes more interfaces and prevents dislocation from moving and grain boundary from sliding, thereby improving the hardness of the film.[21] When nitrogen flow rate exceeds a critical value, the volume fraction of Ti(C,N) nanocrystallines decreases and more sp^2C–N bonds are formed, which reduces the film hardness.[22]

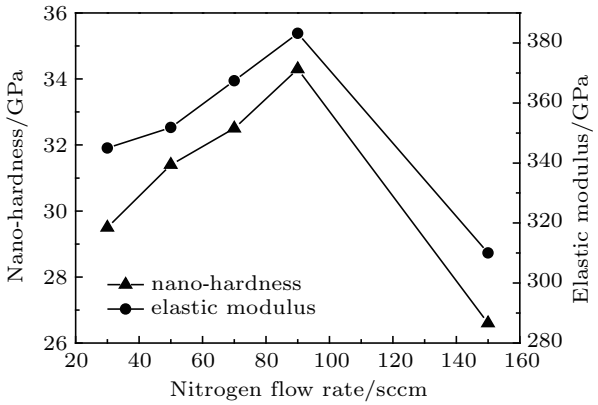


Fig. 8. Nano-hardness and elastic modulus of Ti–C–N films versus nitrogen flow rate.

4. Conclusion

Ti and N co-doped DLC films are prepared by pulsed bias arc ion plating under various nitrogen flow rates. It is found that nitrogen flow rate has significant effects on the composition, microstructure, and mechanical properties of the film. XPS, XRD, Raman analyses confirm the formation of composite structure with Ti(C,N) crystalline phase imbedded in an amorphous carbon matrix. With the increase of nitrogen flow rate, the N–Ti bonding fraction reduces and the N–C bonding fraction increases. The Ti(C,N) peak exhibits low intensity at a high nitrogen flow rate. Nano-hardness values of Ti–C–N films increase from 29.5 GPa to 34.3 GPa as the nitrogen flow rate increases from 30 sccm to 90 sccm, then decreases with the further increase of nitrogen flow rate due to more sp^2 C–N bonds in the film.

References

[1] Zhang G, Li B, Jiang B, Yan F and Chen D 2009 *Appl. Surf. Sci.* **255** 8788
[2] Shafiq M, Hassan M, Shahzad K, Qayyum A, Ahmad S, Rawat R S and Zakaullah M 2010 *Chin. Phys. B* **19** 012801
[3] Cheng Y and Zheng Y F 2007 *Surf. Coat. Technol.* **201** 4909
[4] Lu Y H, Wang J P and Shen Y G 2009 *Appl. Surf. Sci.* **255** 7858
[5] Tsotsos C, Baker M A, Polychronopoulou K, Gibson P N, Giannakopoulos K, Polycarpou A A, Böbel K and Rebholz C 2010 *Thin Solid Films* **519** 24

[6] Martínez-Martínez D, López-Cartes C, Justo A, Fernández A and Sáchez-López J C 2009 *Solid State Sci.* **11** 660
[7] Barshilia H C, Prakash M S, Sridhara Rao D V and Rajam K S 2005 *Surf. Coat. Technol.* **195** 147
[8] Lu Y H and Shen Y G 2007 *Appl. Phys. Lett.* **90** 221913
[9] Chen R, Tu J P, Liu D G, Mai Y J and Gu C D 2011 *Surf. Coat. Technol.* **205** 5228
[10] Lin G Q, Zhao Y H, Guo H M, Wang D Z, Dong C, Huang R F and Wen L S 2004 *J. Vac. Sci. Technol. A* **22** 1218
[11] Zhang M, Lin G Q, Dong C and Wen L S 2007 *Acta Phys. Sin.* **56** 7300 (in Chinese)
[12] Stüber M, Leiste H, Ulrich S, Holleck H and Schild D 2002 *Surf. Coat. Technol.* **150** 218
[13] Zhou F, Adachi K and Kato K 2006 *Thin Solid Films* **514** 231
[14] Guemmaz M, Moraitis G, Mosser A, Khan M A and Parlebas J C 1997 *J. Phys.: Condes. Matter* **9** 8453
[15] Johansson L I, Johansson H I P and Håkansson K L 1993 *Phys. Rev. B* **48** 14520
[16] Wang Q, Zhou F, Zhou Z, Yang Y, Yan C, Wang C, Zhang W J, Li L K Y, Bello I and Lee S T 2012 *Surf. Coat. Technol.* **206** 3777
[17] Levi G, Kaplan W D and Bamberger M 1998 *Mater. Lett.* **35** 344
[18] Robertson J 2002 *Mater. Sci. Eng. R* **37** 129
[19] Chu P K and Li L 2006 *Mater. Chem. Phys.* **96** 253
[20] Zhang S, Zeng X T, Xie H and Hing P 2000 *Surf. Coat. Technol.* **123** 256
[21] Vepřek S and Reiprich S 1995 *Thin Solid Films* **268** 64
[22] Li H K, Lin G Q and Dong C 2010 *Acta Phys. Sin.* **59** 4296 (in Chinese)